frontiers in Materials

ORIGINAL RESEARCH
published: 05 July 2018
doi: 10.3389/fmats.2018.00035

Targeted Methotrexate Prodrug Conjugated With Heptamethine Cyanine Dye Improving Chemotherapy and Monitoring Itself Activating by Dual-Modal Imaging

Sanpeng Li[1,2†], Zhihong Sun[1†], Xiaoqing Meng[1,2], Guanjun Deng[1,2], Jiali Zhang[1,2], Kui Zhou[3], Wenjun Li[1], Lihua Zhou[1], Ping Gong[1,4] and Lintao Cai[1*]*

[1] Guangdong Key Laboratory of Nanomedicine, CAS Key Lab for Health Informatics, Shenzhen Engineering Laboratory of Nanomedicine and Nanoformulations, Shenzhen Institutes of Advanced Technology (SIAT), Chinese Academy of Sciences, Shenzhen, China, [2] University of Chinese Academy of Sciences, Beijing, China, [3] Department of Laboratory Medicine, Peking University Shenzhen Hospital, Shenzhen, China, [4] State Key Laboratory of Chemo/Biosensing and Chemometrics, Hunan University, Changsha, China

OPEN ACCESS

Edited by:
Alexander A. Shtil,
Russian Cancer Research Center NN Blokhin, Russia

Reviewed by:
Eunha Kim,
Ajou University, South Korea
Rajendra K. Singh,
Dankook University, South Korea

***Correspondence:**
Ping Gong
ping.gong@siat.ac.ac
Lintao Cai
lt.cai@siat.ac.cn

[†] These authors have contributed equally to this work.

Specialty section:
This article was submitted to Biomaterials, a section of the journal Frontiers in Materials

Received: 05 January 2018
Accepted: 18 May 2018
Published: 05 July 2018

Citation:
Li S, Sun Z, Meng X, Deng G, Zhang J, Zhou K, Li W, Zhou L, Gong P and Cai L (2018) Targeted Methotrexate Prodrug Conjugated With Heptamethine Cyanine Dye Improving Chemotherapy and Monitoring Itself Activating by Dual-Modal Imaging. Front. Mater. 5:35. doi: 10.3389/fmats.2018.00035

Theranostic prodrug plays a vital role in reducing the side effects and evaluating the therapeutic efficiency of prodrug *in vivo.* In particular, small conjugate-based theranostic prodrugs have attracted much attention because of their clear and simple structures. In this work, we synthesized a novel tumor-targeting and glutathione-activated conjugate-based theranostic prodrug (Cy-SS-MTX). The prodrug was constructed by conjugating Cy (IR780) to methotrexate (MTX) via a disulfide bond. The Cy dye as targeting molecule bring prodrug to cancer cells and then the prodrug was activated by the high levels of glutathione in tumor. In cell experiments, the results showed the excellent ability of prodrug to target tumor. Meanwhile, the prodrug apparently improved the anti-tumor ability and hugely reduced toxicity of free MTX on normal cells. Furthermore, owing to intramolecular charge transfer between Cy and MTX, the Cy structure in the prodrug showed an absorption peak at 654 nm in UV-Vis spectroscopy. However, when the disulfide bond of prodrug was broken by glutathione, a new UV-Vis absorption peak at 802 nm of Cy structure in prodrug was arised. At the same time, the fluorescence (FL) emission peak at 750 nm (excitation at 640 nm) would turn into 808 nm (excitation at 745 nm). What's more, the photoacoustic (PA) signal with excitation at 680 and 808 nm also changed. The experimental results *in vivo* showed that the prodrug has been successfully utilized for real-timely tracking MTX activation by FL and PA imaging upon near infrared laser excitation and cancer targeting therapy. Our studies further encourage application of small conjugate-based prodrug based on tumor-targeted heptamethine cyanine dye as reporter group for targeted therapy and real-timely tracking activation of drug.

Keywords: small conjugate-based prodrug, heptamethine cyanine dye, dual-modal imaging, monitoring prodrug activation, theranostic, targeting therapy

INTRODUCTION

Traditional chemotherapeutic drugs used to treat cancer are limited due to the high toxicity and nonselectivity on normal tissue (Li et al., 2014; Zhao et al., 2015; Bi et al., 2016; Gao et al., 2017; Kang et al., 2017; Zhou et al., 2017). To reduce the side-effects and improve the therapeutic efficiency, prodrugs have been designed and synthesized (Rautio et al., 2008; Huttunen et al., 2011; Abet et al., 2017). Prodrugs relates to biologically inert derivatives of drug molecules that undergo chemical modification (Hu et al., 2013; Lee et al., 2017). They are inactive prodrugs in normal tissues, but can be converted into active drugs specifically via exogenous or endogenous activating approaches (Penet et al., 2012; Tam et al., 2016; Li B. et al., 2017). The endogenous activating approaches rely on tumor microenvironment, such as high concentration of biothiols, enzymes overexpressed in tumor cells, low pH values and hypoxia (Zheng et al., 2016; Han et al., 2017; He et al., 2017; Li Y. et al., 2017), while external activating methods include light, temperature, and other external stimuli (Don et al., 2017; Liu et al., 2017). The prodrug strategy can achieve site-selective activation, decrease toxicity and improve therapeutic index. Since it is very important to monitor the activation of prodrugs and evaluate the therapeutic efficiency of prodrugs, theranostic prodrugs which possess covalently attached drugs and imaging units can real-timely monitor the biodistribution and activation of prodrugs in cancer therapy *in vivo* have been a hot area of prodrugs research (Liu et al., 2013; Gangopadhyay et al., 2017; Hu et al., 2017; Morsy et al., 2017).

Recently, small conjugate-based theranostic prodrugs (SCTPs) which are prepared by the covalent conjugation drugs and contrast agents with linkers have received much attention for cancer treatment and diagnosis. They can be easily modified to get desired chemotherapeutic efficacy because of their structural architectures are relatively clear, simple and biocompatible (Kumar et al., 2015; Liu et al., 2015). Comparing to nanoparticle-based prodrugs, SCTPs can be easily cleared by excretory system (Lim et al., 2014; Tibbitt et al., 2016). However, it is still challenging to design SCTPs which have an excellent ability of targeting tumor, monitor the location and activation of prodrug, improve the therapeutic effect simultaneously. Nowadays, heptamethine cyanine dyes have been widely used for tracking prodrug activation due to their excellent optical properties in the near–infrared (Wu et al., 2014, 2015a; Chao et al., 2016; Sun et al., 2016; Ye et al., 2016; Atchison et al., 2017). What's more, some of them present the excellent tageting ability to tumor due to overexpression of certain types of organic anion transport peptide in cancer cell (Wu et al., 2015b; Shi et al., 2016; Guan et al., 2017; Meng et al., 2017). Henren, it is a good strategy to use heptamethine cyanine dye as reporter group in designing SCTPs.

Herein, a glutathione-activated SCTPs (Cy-SS-MTX) was constructed by conjugating Cy (IR780) to methotrexate (MTX) via a disulfide bond (**Figure 1A**). The prodrug possessed tumor targeting ability (Cy) and could be activated by overexpressed glutathione in tumor. So it would improve anti-tumor efficiency of MTX to cancer cells and reduce toxicity of MTX to normal cells. Owing to intramolecular charge transfer in Cy and MTX, the Cy group in the prodrug showed a UV-vis absorption peak at 654 nm and fluorescence emission peak at 750 nm. However, when the disulfide bond of prodrug was broken by the high level of glutathione, the optical properties of Cy changed. A new UV-vis absorption peak at 802 nm and fluorescence emission peak at 808 nm arised, and at the same time the photoacoustic signal also changed. We believed the Cy-SS-MTX could specifically target the tumor and the process of prodrug activation could be real-timely tracked by fluorescence/photoacoustic dual-modal imaging.

EXPERIMENTAL

Materials and Instruments

Heptamethine cyanine dye IR780 and Methotrexate (MTX) were purchased from sigma company (USA). Bis-(2-aminoethyl) disulfidedihydrochloride and Triethylamine were obtained from J&K scientific Ltd. (China). N,N'-Dicyclohexyl carbodiimide (DCC), 1-hydroxy-5-pyrrolidinedione (NHS) and 4-(dimethylamino)-pyridin (DMAP) were purchased from Shanghai Aladdin Bio-Chem Technology Co., Ltd. Cell Counting Kit-8, Mitochondria Staining Kit and DAPI were purchased from sigma company (USA). All solvents and reagents were analytical grade and used without further purification. ^{1}H NMR and ^{13}C NMR spectra were recorded with a Bruker 400 MHz. The high-resolution mass spectra (HR-MS) were measured on a Bruker Micro TOF II 10257 instrument. UV-visible Spectra was recorded on Varian Cary 50 spectrometer. Fluorescence spectra were recorded on FP-600. Confocal laser scanning microscopy (CLSM) was performed on an Olympus FV1000 confocal (red laser 10 mW).

The Synthesis of Cy-SS-MTX

Firstly, the Cy-SS was made. Cystaminedihydrochloride (6.97 mg) was dissolved in anhydrous DMF (5 ml) with TEA (2.1 μl). Then, IR780 (10 mg) dissolved in anhydrous DMF (500 μl) was drop-wise added to the above solution under N2 atmosphere at room temperature. The solvent was evaporated under reduced pressure to get crude product Cy-SS after 4 h later. The product was further purified by silica gel column chromatography with dichloromethane and methanol. Secondly, Cy-SS-MTX was made by amido linkage. Under N_2 atmosphere, the MTX (50 mg) activated by NHS (12.7 mg), DCC (22.7 mg), and DMAP (21.5 mg) was added to Cy-SS (55 mg) dissolved in DMF. The reaction was going overnight at room temperature. Finally, the Cy-SS-MTX was purified by silica gel column chromatography with dichloromethane and methanol. Yield: 48%. The control group Cy-CC-MTX was also made in using same way. Yield: 46%. The structures were analyzed by TOF Mass Spectrum and NMR respectively.

The Analysis of Optical Properties in Cy-SS-MTX

Cy-SS-MTX was dissolved in mixture solution of DMSO and PBS (V/V = 4:6). Normalized UV-Vis absorption of Cy-SS-MTX (5 μM) in the above mixture solution with or without GSH (0 /1/5/10/15/25/35/50/75/100/150/250 μM) was obtained.

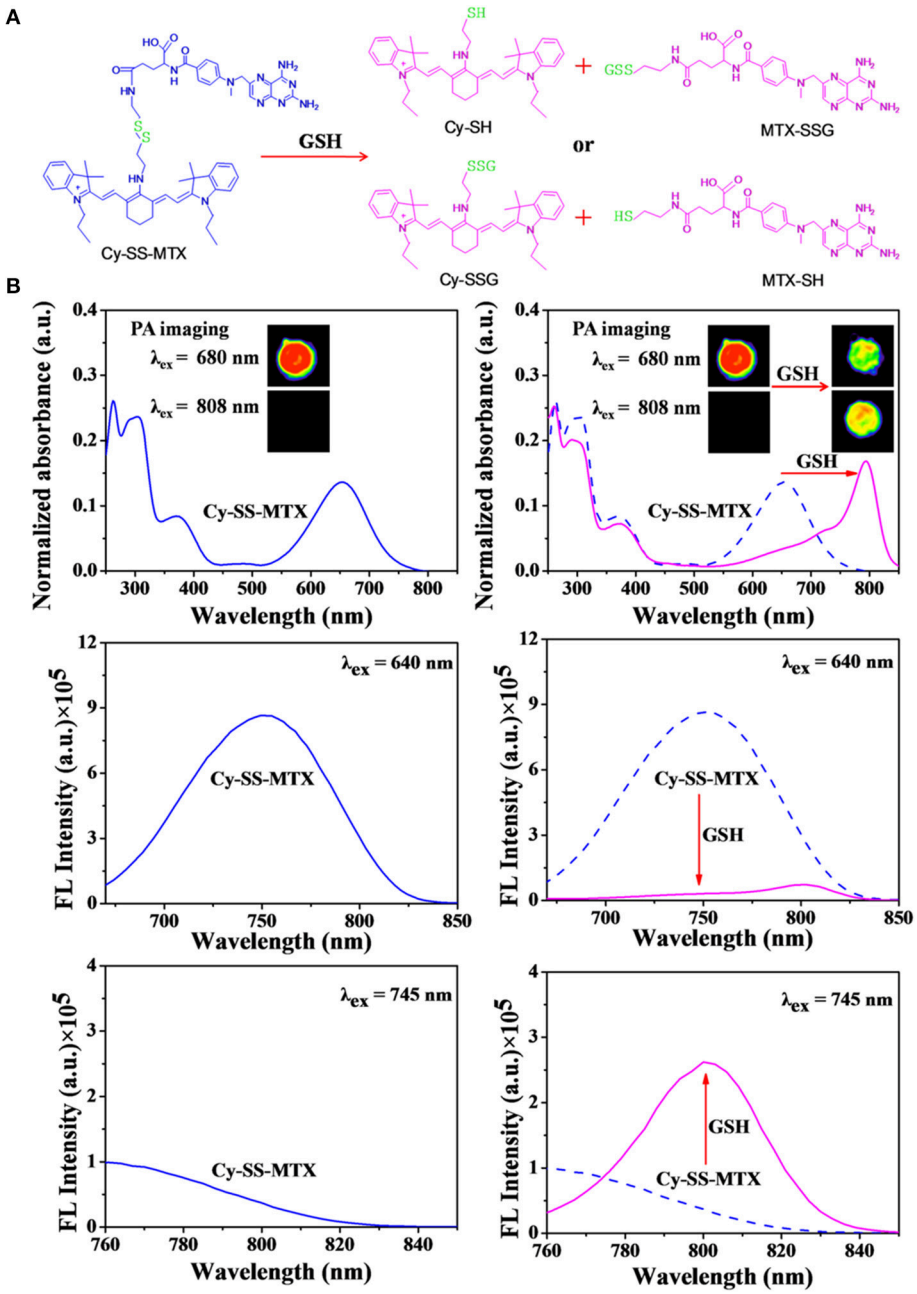

FIGURE 1 | (A) Schematic the two ways of GSH activation in theranostic prodrug Cy-SS-MTX in cancer cells. **(B)** The changes in PA imaging, UV-Vis absorption and fluorescent characteristics of Cy-SS-MTX in the presence of GSH or not. The PA imaging upon excitation at 680/808 nm and fluorescence characteristics upon excitation at 640/745 nm.

All samples were measured by Varian Cary 50 spectrometer after incubation for 15 min at 37°C. To obtain fluorescent characteristics of Cy-SS-MTX, (5 μM), the solution was added GSH (0/5/25/50/75/125/175/250/375/500/750/1,250 μM) and cultivated 30 min at 37°C. Then, mixture solutions were excited by 640 and 745 nm respectively. The Fluorescence response of drug carrier with various thiol-containing matters and amino acids was also measured by the above way. In photoacoustic imaging experiments, firstly, Cy-SS-MTX excited by 680 and 808 nm were mixed with GSH (0/15/150/750/1,500 μg/ml). The value of concentration of Cy-SS-MTX was 15 μg/ml. Secondly, time dependence of photoacoustic imaging of Cy-SS-MTX was made in the presence of GSH (1,500 μg/ml). The value of concentration of Cy-SS-MTX was also 15 μg/ml. The optical properties of control group Cy-CC-MTX were also studied under the same experiments.

Cell Culture

In a humidified atmosphere with 5% CO_2 incubator, the cell (cancer cell: A549/MCF-7/SKOV-3, normal cell: MCF-10A/L02) was cultured in DMEM medium (Gibco, Grand Island, NY, USA) containing 10% (v/v) fatal bovine serum (FBS), 100 U/ml penicillin and 100 μg/ml streptomycin at 37°C. The above cells were purchased from the cell repository of Chinese Academy of Sciences.

The Cytotoxicity of Cy-SS-MTX

The A549/MCF-7/SKOV-3/MCF-10A cells were seeded in 96-well plate (1×10^4 cells) and incubated overnight at 37°C in a humidified atmosphere with 5% CO_2. As described above, the culture medium was replaced with 200 μL medium contained 0.01/0.1/1/5/10/15/25/50 μM MTX of Cy-SS-MTX/Cy-CC-MTX. After 4 h, the medium was rinsed again with 200 μL fresh culture medium. After another 24 h of incubated in the dark, the cell viability was evaluated by CCK-8 assay. The relative marker of apoptosis and cell cycle arrest were induced by Cy-SS-MTX, which were detected by western blotting analysis.

In Vitro Cell Uptake of Cy-SS-MTX

MCF-7 and L02 cell were seeded into 8-well chambered coverglass (Lab-Tek, Nunc, USA) at a density of 1×10^4 per well respectively. After 24 h, the culture medium was replaced by new medium containing 5 μM Cy-SS-MTX/Cy-CC-MTX and placed in incubator for 4 h. After that, the cells were washed thrice with phosphate buffer saline (PBS). Then, the cells were stained by DAPI for 15 min and Mito Tracker excited at 488 nm for 30 min respectively. Finally the cells were observed using confocal (Leica TCS SP5, GER). DAPI was excited at 405 nm. Cy-SS-MTX/Cy-CC-MTX was excited at 633 nm.

For further cellular uptake analysis, normal cells: MCF-10A, L02 and cancer cells: MCF-7, HepG2 cells were seeded into 6-well plates and incubated 24 h. Then, the cells were washed thrice with PBS and added into the new medium containing 5 μM Cy-SS-MTX/Cy-CC-MTX. After 4 h, the cells were collected and analyzed by FACS CantoTM II Gallios flow cytometer (BD Biosciences, red laser 23.74 mW). The above cells were purchased from the cell repository of Chinese Academy of Sciences.

Animals and Tumor Model

All experimental procedures involving animals were approved by the Ethics Committee of Shenzhen Institutes of Advanced Technology, Chinese Academy of Sciences (SIAT). The research project in the acknowledgment (NSF of China, 31571013) which included this study has acquired the approval of the Ethics Committee of SIAT (The license number for Ethics, SIAT-IRB-150304-YYS-CLT-A0131-2). The research project (NSF of china 31571013) is ongoing (2016/1/1-2019/12/31). Female BALB/c nude mice (5 weeks old and weighed 18–20 g) were purchased from Vital River Laboratory Animal Technology Co. Ltd (Beijing, China). To set up the tumor model, MCF-7 cells (0.5×10^6) in 0.2 mL of saline solution were administered by subcutaneous injection into the hind legs region.

In Vivo Dual-Model Imaging Monitoring the Activation of Prodrug

The nude mice were divided into two groups (three per group) randomly. Mice with tumor sizes about 300 mm^3 in volume were used and intravenously injected with 100 μl Cy-SS-MTX/Cy-CC-MTX (80 μg/ml). For fluorescence imaging, the above prodrug carriers were excited with two laser wavelengths at 640 and 745 nm. For photoacoustic imaging, the laser wavelengths were changed to 680 and 808 nm. The semiquantitative analysis of fluorescence and photoacoustic imaging were taken at 0.5/1/4/8/24 h after injection with IVIS imaging system (mercury lamp 150 W) and Endra Nexus 128 imaging system. Then, the distribution of the Cy-SS-MTX was measured at 1 or 24 h post-injection in *ex vivo* organs (heart, liver, spleen, lung, kidney, and tumor).

RESULTS AND DISCUSSION

Synthesis and Characterization of Cy-SS-MTX

The Cy-SS-MTX was synthesized in a two-step process (Supplementary Figure 1). Firstly, the Cy-SS was obtained by the reaction of Cy with cystamine in anhydrous DMF. The reaction mixture was reacted at room temperature for 6 h under Nitrogen atmosphere. The solvent was removed under reduced pressure and then the crude product was purified by chromatography. Secondly, the Cy-SS was conjugated to the MTX by amido linkage to obtain the Cy-SS-MTX in DMF. MTX was activated with DCC, NHS, and DMAP for 3 h in DMF before used. After 24 h, the solvent was removed under reduced pressure and the product was purified by chromatography. The molecular weights and structures of products were confirmed by mass spectrometry and NMR respectively. Cy-SS $[M+H]^+$ m/z found 655.3866; Cy-SS-MTX $[M+H]^+$ m/z found 1091.5483; Cy-CC $[M+H]^+$ m/z found 619.4728; Cy-CC-MTX $[M+H]^+$ m/z found 1055.6340 (Supplementary Figure 10). ^1H NMR and ^{13}C NHR (Bruker 400 MHz) of below materials Cy-SS and Cy-CC were dissolved in Methanol-D4. Cy-SS-MTX and Cy-CC-MTX were dissolved in DMSO-D6 (Supplementary Figure 11). The above results certificated that the Cy-SS-MTX was made successfully.

The UV-Vis spectrum of prodrug Cy-SS-MTX was recorded. It was evident that when Cy was covalently bound to MTX, the absorption peak of Cy exhibited a blue shift from 802 to 654 nm. A remarkable spectral shift by modulating the pull–push conjugated π-electron system (ICT process) between Cy and MTX (electron drawing group) made a 148 nm blue shift of Cy in UV-Vis absorption (Supplementary Figure 2A). When Cy was connected with MTX covalently, MTX (electron drawing group) could largely absorb the electrons in N atom of cystamine. Meanwhile, the electrons of N atom of cystamine which transfer to Cy would be reduced. Therefore the pull–push π-conjugation system in the tricarbocyanine chromophore (between N atom of cystamine and Cy) is obviously shortened, resulting in a large hypsochromic shift of Cy in UV-Vis absorption. Furthermore, with adding GSH, the absorption of Cy group in prodrug at

802 nm was gradually increasing, but the absorption at 654 nm was declining (**Figure 2A**). More importantly, the above analysis showed the ratio absorption of prodrug in 802/654 nm exhibited a good linear relationship with GSH concentration (**Figure 2D**). However, the UV-Vis absorption of Cy-CC-MTX had no similar results (Supplementary Figures 2B,3A).

The fluorescent spectrum of Cy-SS-MTX was then studied. Two different excitation wavelengths (640/745 nm) were chosen to excite Cy group in prodrug. We could observed that the Cy group in prodrug had a strong fluorescent emission peak at 750 nm (λ_{ex} = 640 nm) and very weak fluorescent emission peak at 808 nm (λ_{ex} = 745 nm). However, in the existence of GSH, the prodrug exhibited contrary fluorescent property that it had a strong fluorescent emission peak at 808 nm (λ_{ex} = 745 nm) and weak fluorescent signal peak at 750 nm (λ_{ex} = 640 nm) (**Figure 1B**). Then, with increasing GSH, the intensity of fluorescence of Cy group in prodrug at 750 nm emission peak (λ_{ex} = 640 nm) would gradually decline (**Figures 2B,E**), while the intensity at 808 nm emission peak (λ_{ex} = 745 nm) was increasing (**Figures 2C,F**). On the contrary, the fluorescent signals of Cy-CC-MTX kept almost unchanging when adding different GSH levels (Supplementary Figures 3B,C). Thus, a remarkable change of fluorescent spectrum shown in prodrug Cy-SS-MTX reacted with GSH could monitor activation of prodrug. Subsequently, the responses of prodrug to other biologically relevant matters such as amino acids and ions were investigated. The results exhibited that biothiol could break disulfide bond in prodrug, but the other matters had no responding (Supplementary Figures 4A,B). Besides, the reaction kinetics of prodrug with GSH was investigated. While the intensity of prodrug fluorescent emission at 808 nm peak (λ_{ex} = 745 nm) would gradually increase within 30 min, the

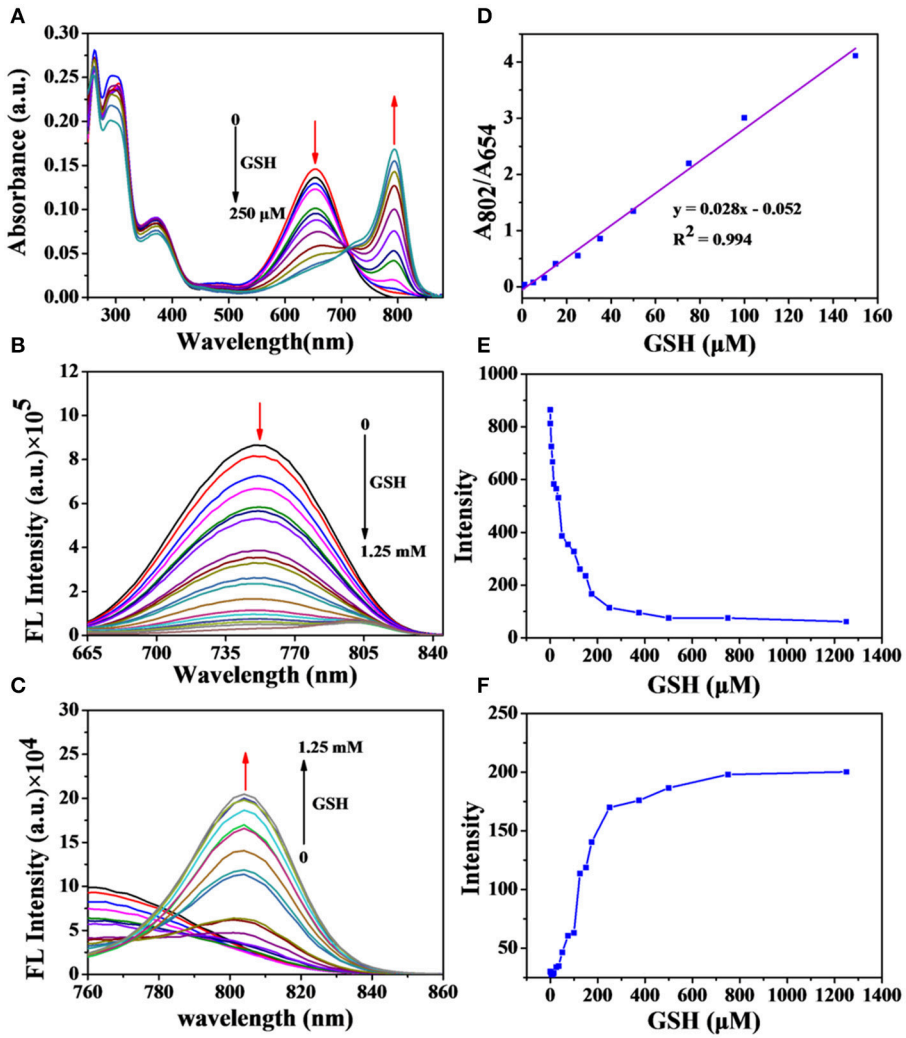

FIGURE 2 | (A) UV-Vis absorption changes of Cy-SS-MTX (5 μM) in the presence of GSH in the DMSO/PBS (1/1, v/v, PH = 7.4). Fluorescence spectra responses of Cy-SS-MTX (5 μM) to GSH (λ_{ex} = 640 nm/λ_{em} = 750 nm **(B)**, λ_{ex} = 745 nm/λ_{em} = 808 nm **(C)**. **(D)** The rate value of absorption of Cy-SS-MTX in 802 and 654 nm as function of GSH shown in **(A)**. The value of fluorescent intensity at 750 nm **(E)** and 808 nm **(F)** of Cy-SS-MTX as function of GSH shown in **(B,C)** respectively.

control group of Cy-CC-MTX had little change (Supplementary Figure 4C).

In the PA imaging analysis, we chose two kinds of excitation wavelengths (680/808 nm) to excite Cy group in Cy-SS-MTX, according to UV-vis absorption of Cy-SS-MTX. The PA intensity of Cy-SS-MTX excited by 680 nm was higher than excited by 808 nm (**Figure 3A**). With adding GSH, the signal of PA imaging excited by 808 nm was gradually increasing, while the signal excited by 680 nm was declining (**Figures 3C,D**). However,the control group of Cy-CC-MTX had no similar change (Supplementary Figure 5B). In the real-time PA monitoring prodrug activation, the signal of PA imaging excited by 808 nm gradually increased within 60 min, but the signal excited by 680 nm declined (Supplementary Figure 7A). However, the group of Cy-CC-MTX also had little signal change at the same condition (Supplementary Figure 7B). Moreover, the intensity of PA imaging of Cy-SS-MTX excited by 680/808 nm both exhibited a good linear relation with the concentration of Cy-SS-MTX (**Figure 3B**), GSH and time of reaction (Supplementary Figures 6, 8). *In vitro* the results demonstrated that the activation of prodrug Cy-SS-MTX could also be monitored by PA imaging.

Cellular Uptake of Cy-SS-MTX

The cellular uptake of prodrug Cy-SS-MTX was monitored by CLSM and flow cytometry. Cy-SS-MTX and Cy-CC-MTX were all co-cultured with cells (L02 normal cells, MCF-7 cancer cells) respectively. After 30 min, the cells were stained with Mito Tracker. From the results that there were all little red fluorescence from L02 cells while much from MCF-7 cells in Cy-SS-MTX and Cy-CC-MTX, we could conclude that Cy-SS-MTX and Cy-CC-MTX both showed the ability of excellent tumor-targeting. Besides, the result also revealed that the green signals of mitochondria (excited by 365 nm) were mainly overlapped with the red ones exhibited by Cy-SS-MTX/Cy-CC-MTX, which indicated that the prodrug Cy-SS-MTX was located in mitochondria preferentially (**Figure 4A**). To further certificate the tumor-targeting ability of Cy-SS-MTX/Cy-CC-MTX, flow cytometry experiment was carried out in the cancer cells (MCF-7, Hepg2), the normal cells (L02) and MCF-10A used to represent the normal breast cell model. The flow cytometry showed that the fluorescence intensities in cancer cells were 10 times higher than the normal cells at same condition (**Figure 4B**). The results were in accordance with the CLSM and further showed the excellent tumor-targeting ability of prodrug.

Subsequently, to analyze the activation of prodrug Cy-SS-MTX in cancer cells *in vitro*. MCF-7 cells were co-cultured with Cy-SS-MTX/Cy-CC-MTX. Images were obtained at 0/3/6 h after cultivation for 30 min. The cells showed that there were gradual declining red fluorescence signals in the experiment of Cy-SS-MTX, but red fluorescence signals of Cy-CC-MTX group kept almost unchanging (**Figure 5**). The reasons for explaining that, for one thing, there was only 633 nm chosen for excitation because of restriction of CLSM, for another thing, when the prodrug Cy-SS-MTX was activated by high GSH level in cancer cell, the fluorescent signals excited by 640 nm would disappear (**Figure 2B**). However, the above trend did not be observed in Cy-CC-MTX group because it could not be activated by GSH. Comparing changes of fluorescence imaging between Cy-SS-MTX and Cy-CC-MTX, we could conclude that activation of prodrug could be observed by FL imaging.

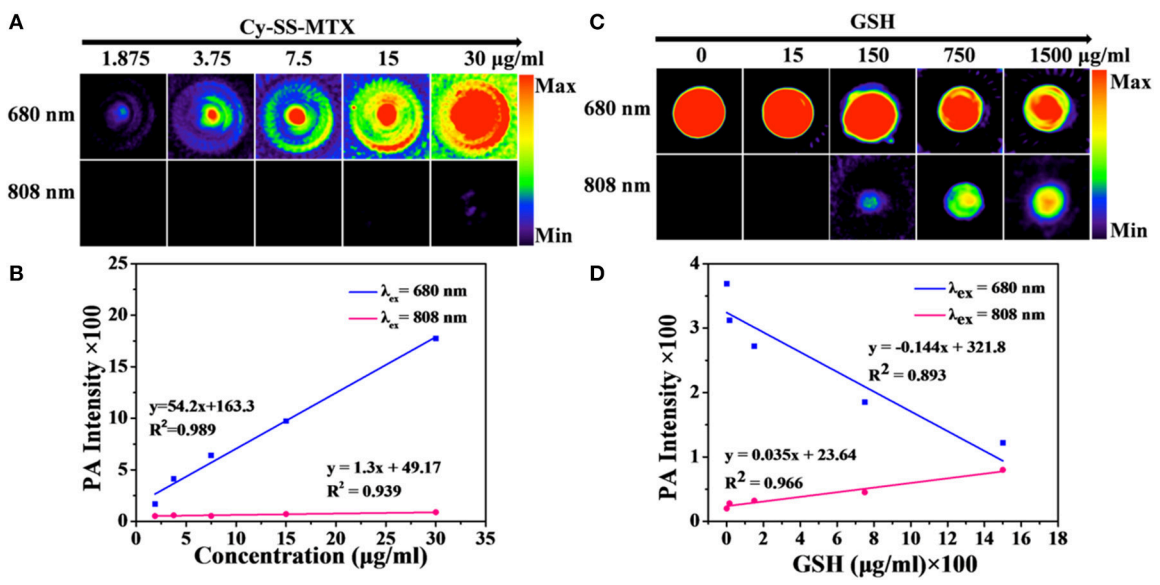

FIGURE 3 | (A) PA imaging of Cy-SS-MTX with varying concentration of Cy-SS-MTX upon excitation at 680 and 808 nm respectively. **(B)** The intensity of PA imaging with varying concentration of Cy-SS-MTX shown in **(A)**. **(C)** PA imaging responses of Cy-SS-MTX to GSH upon excitation at 680 and 808 nm respectively. **(D)** The intensity of PA imaging with varying concentration of Cy-SS-MTX shown in **(C)**.

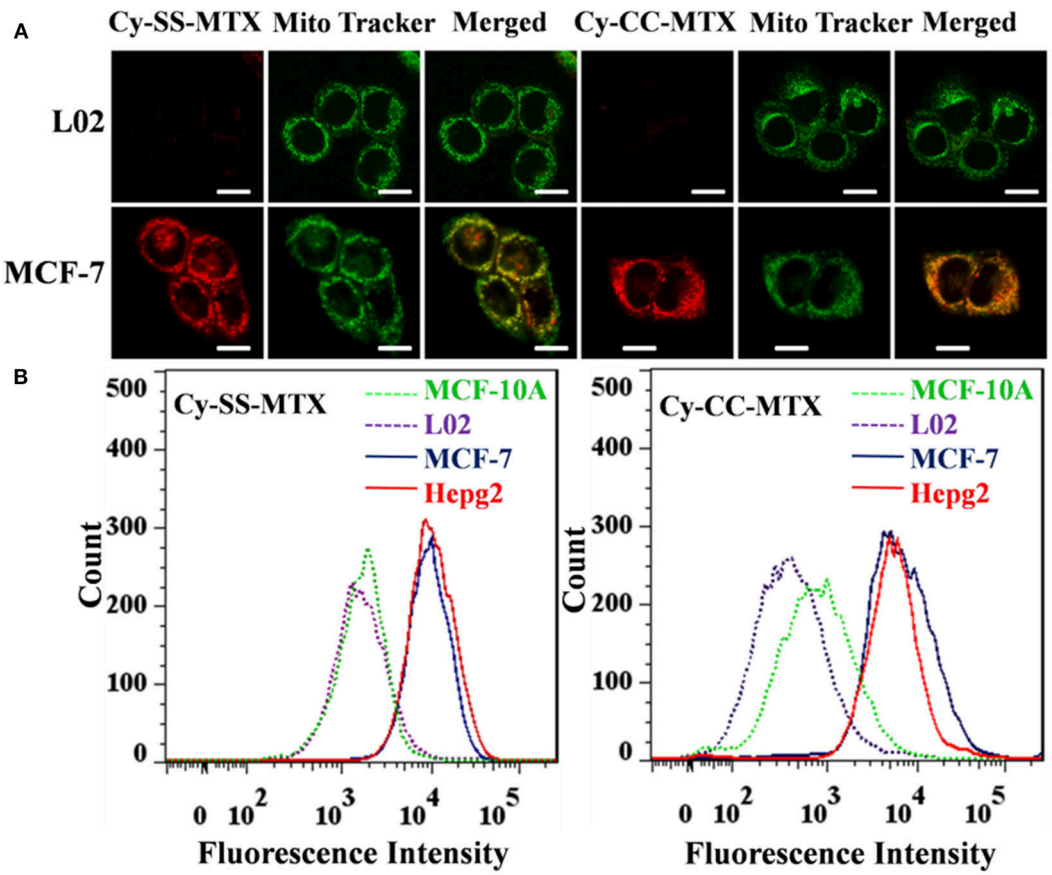

FIGURE 4 | (A) Fluorescence confocal microscope images of L02 normal cells and MCF-7 cancer cells cultured with Cy-SS-MTX/Cy-CC-MTX (5 μM) for 0.5 h respectively. Images were obtained using an excitation wavelength of 633 nm (Cy-SS-MTX/Cy-CC-MTX) and 488 nm (Mito). Scale bar, 10 μm. **(B)** Flow cytometry analysis of cellular uptake of Cy-SS-MTX/Cy-CC-MTX. Normal cells: L02. Breast Cancer Progression Cell Line Model: MCF-10A. Cancer cells: MCF-7, Hepg2.

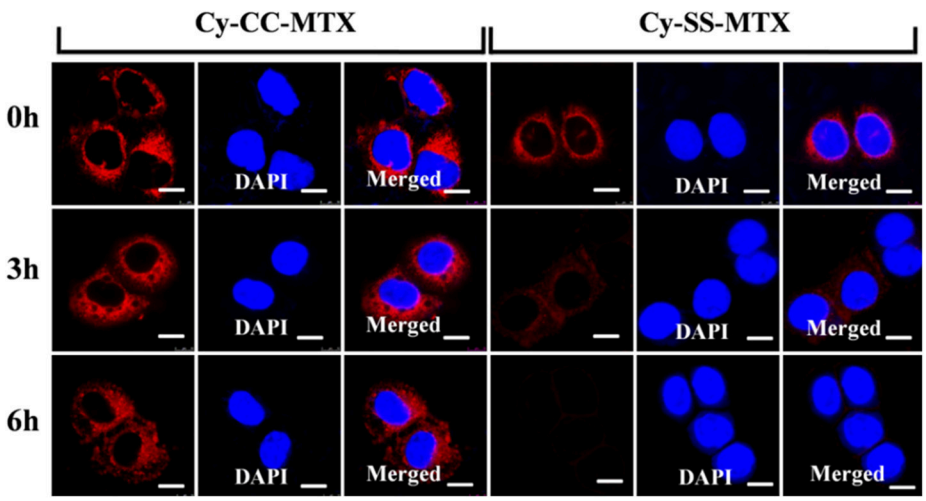

FIGURE 5 | Time-dependent Fluorescence confocal microscope images of MCF-7 cancer cells for tracking the activation of prodrug Cy-SS-MTX. Images were obtained at 0/3/6 h after cultivating Cy-SS-MTX or CY-CC-MTX (5 μM) with cells for 30 min. (λ_{ex} = 633 nm for Cy-SS-MTX/Cy-CC-MTX and λ_{ex} = 405 nm for DAPI). Scale bar, 10 μm.

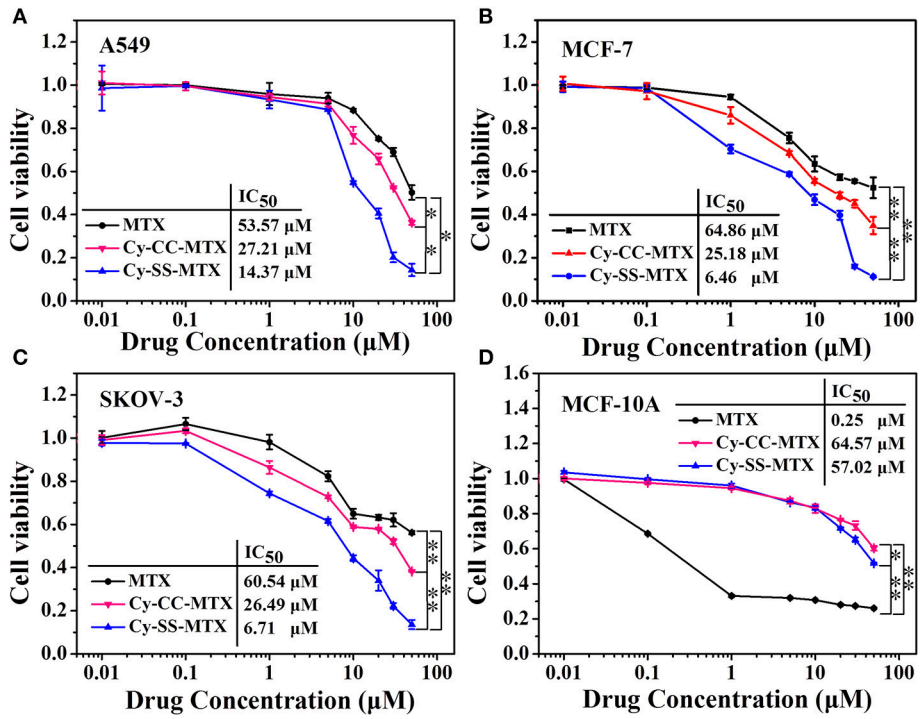

FIGURE 6 | The cytotoxicity of MTX, Cy-SS-MTX, and Cy-CC-MTX on cancer cells **(A–C)**. The cytotoxicity of them on MCF-10A cells **(D)**. The culture medium of three groups contained 0.01/0.1/1/5/10/20/30/50 μM MTX respectively. (*denotes $P < 0.05$, **denotes $P < 0.01$ significant difference).

Anti-Tumor Efficiency Study

To investigate the anti-tumor efficiency of prodrug Cy-SS-MTX, four kinds of cells (cancer cell: MCF-7/SKOV-3/A549, Breast Cancer Progression Cell Line Model: MCF-10A) were used in this experiment. For the cancer cells we selected, the IC_{50} values of Cy-SS-MTX were about 5–10-fold smaller than the free MTX (**Figures 6A–C**). For normal cell, the IC_{50} value of Cy-SS-MTX was over 200 fold larger than the free MTX (**Figure 6D**). Compared with the drug MTX, the prodrug showed better anti-tumor efficiency than MTX on the cancer cells but lower toxicity on normal cells at the same molarity of MTX. Undoubtedly, this MTX analog in this design did not change the anti-tumor efficiency because of aminopeptidases within cells (Warnecke et al., 2007; Li et al., 2015; Lin et al., 2015). The Cy group of prodrug could bring MTX to cancer cells more efficiently because the good tumor-targeting of Cy (the targeting ability of Cy did not change after IR780 covalent linking with MTX), that might be the reason of prodrug showing more toxicity to cancer cells and lower toxicity to normal cells. On the contrary, the group of Cy-CC-MTX exhibited bad anti-tumor activity and lower toxicity than Cy-SS-MTX on cancer cells because the uncleavable carbon-carbon covalent bond between Cy and MTX. We also used Western Blot to study the cell cycle arrest and cytotoxic assay in MCF-7 cells. The data of cell cycle arrest and cytotoxic assay also are consistent with MTT. The Cy-SS-MTX could promote the apoptosis and inhibit cell cycle in cancer cells (Supplementary Figure 9). Thus, the prodrug Cy-SS-MTX could effectively reduce toxicity of MTX to normal cells and largely improve the ability of anti-tumor efficiency of MTX.

In Vivo Dual-Model Imaging Monitoring Activation of Prodrug

In order to monitor activation of prodrug Cy-SS-MTX *in vivo*, two groups of mice were injected with Cy-SS-MTX/Cy-CC-MTX via intravenous injection respectively. Within 24 h, the signals of dual-model imaging FL excited by 640/745 nm lasers and PA excited by 680/808 nm lasers were recorded. Then, the distribution of prodrug was measured at 1 and 24 h post-injection in *ex vivo* organs (heart, liver, spleen, lung, kidney and tumor).

In tumor FL imaging, for one thing, we could obtain that the red fluorescent signals of Cy-SS-MTX and Cy-CC-MTX excited by 640 nm reached the maximum at 1 h post-injection, and then the signals would reduce gradually (**Figures 7A,B**). What's more, semiquantitative average FL signals directly showed the above trends (**Figures 7E,F**). The above results indicated that Cy-SS-MTX and Cy-CC-MTX could rapidly target tumor. For another thing, the fluorescent signals of Cy-SS-MTX excited by 745 nm gradually appeared and reached maximum at 8 h. However, there were little fluorescent signals in control group of Cy-CC-MTX excited by 745 nm at the same time. The above data indicated that the Cy-CC-MTX only had an ability of targeting tumor but was not activated with GSH because the structure of disulfide linkage in Cy-SS-MTX could be broken by high GSH level in cancer cells

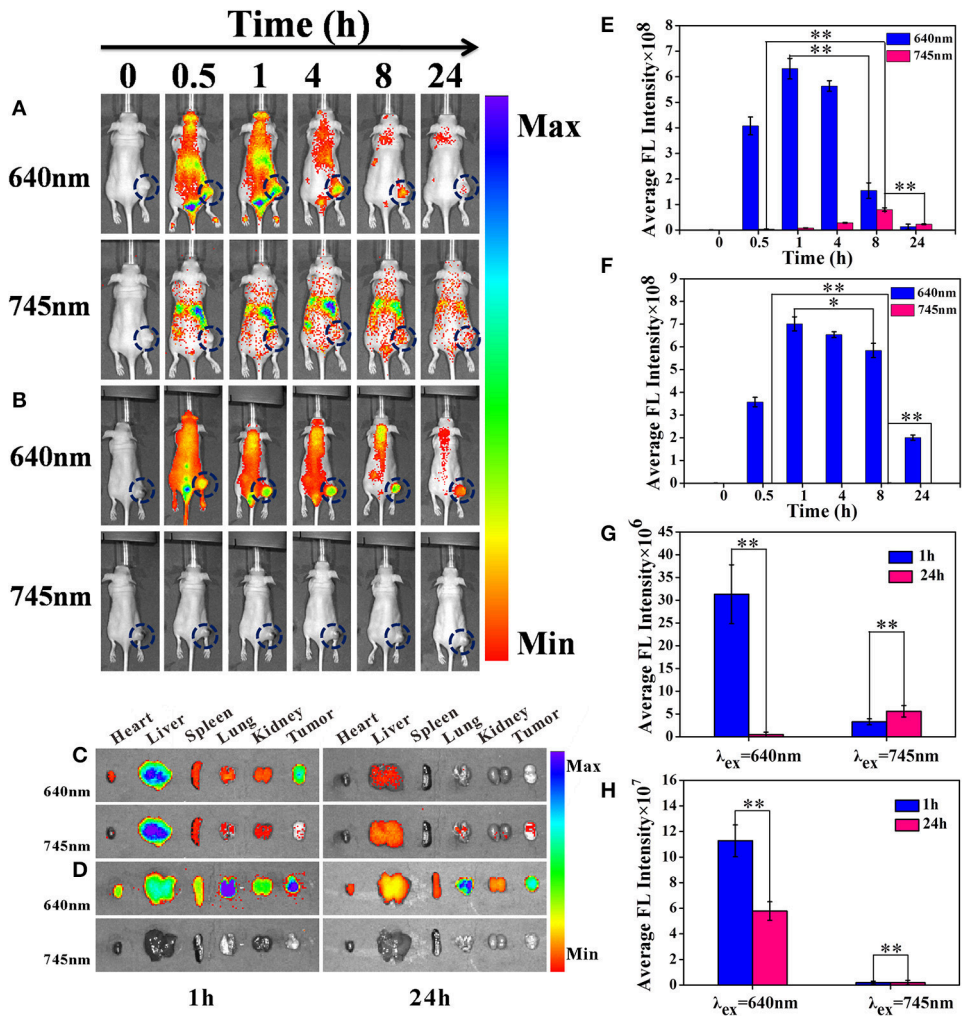

FIGURE 7 | *In vivo* biodistribution and NIRF imaging of Cy-SS-MTX in tumor-bearing mice at 0/0.5/1/4/8/24 h after intravenous injection. **(A)** The groups injected by Cy-SS-MTX excited by 640 nm and 745 nm respectively. **(B)** The groups injected by Cy-CC-MTX excited by 640 and 745 nm respectively. *Ex vivo* NIRF image of normal organs and tumors for the mice injected with Cy-SS-MTX **(C)** Cy-CC-MTX **(D)** at 1 or 24 h post-injection. **(E,F)** Semiquantitative average FL signals in the tumor sites of **(A,B)** respectively. *Ex vivo* fluorescent images of normal organs and tumors excised at 1 and 24 h post-injection with Cy-SS-MTX **(E)** and Cy-CC-MTX **(F)**. **(G,H)** Semiquantitative average FL signals in the tumors sites of **(C,D)** respectively. Note that the samples were all excited by 640 and 745 nm respectively. Red fluorescence excited by 745 nm represents the drug release. (*denotes $P < 0.05$, **denotes $P < 0.01$ significant difference).

in which the MTX prodrug was activated, but carbon-carbon covalent bonds within Cy-CC-MTX had no responding to GSH.

To demonstrate the *in vivo* biodistribution behavior of the Cy-SS-MTX, the mice bearing MCF7 tumor were sacrificed at 1 and 24 h post-injection. Then, the distributions of the prodrug were measured at 1 and 24 h post-injection in *ex vivo* organs (heart, liver, spleen, lung, kidney and tumor). Under the 640 nm laser excitation at 1 h post-injection, the date showed Cy-SS-MTX and Cy-CC-MTX both had a good ability of accumulation in tumor which indicated the good tumor-targeting capacity of the prodrug (**Figures 7C,D**). Under the 745 nm laser excitation, the group of Cy-SS-MTX showed that the fluorescent signals at 24 h was higher than at 1 h, however, there was always little fluorescence in the group of Cy-CC-MTX at measured time. Semiquantitative average FL signals of Cy-SS-MTX and Cy-CC-MTX also directly showed the above trends (**Figures 7G,H**). The biodistribution behavior in *ex vivo* organs indicated that Cy-SS-MTX not only could rapidly target tumor, but also was activated by GSH in the tumor.

Compared to fluorescent imaging, PA imaging is a newly developed biomedical imaging modality with increased imaging depth and improved resolution. PA imaging was developed on the basis of the PA effects of materials with strong light absorbance (Beard, 2011; Zhang et al., 2011; Jeon et al., 2014; Mitcham et al., 2015). Two kinds of lasers (680 and 808 nm) were selected according to the characteristics of Cy-SS-MTX and Cy-CC-MTX absorption in UV-Vis. We obtained the same results like the FL imaging. The signals of PA imaging excited by 680 nm of Cy-SS-MTX/Cy-CC-MTX reached the maximum at 1 h post-injection (**Figures 8A,B**). Semiquantitative

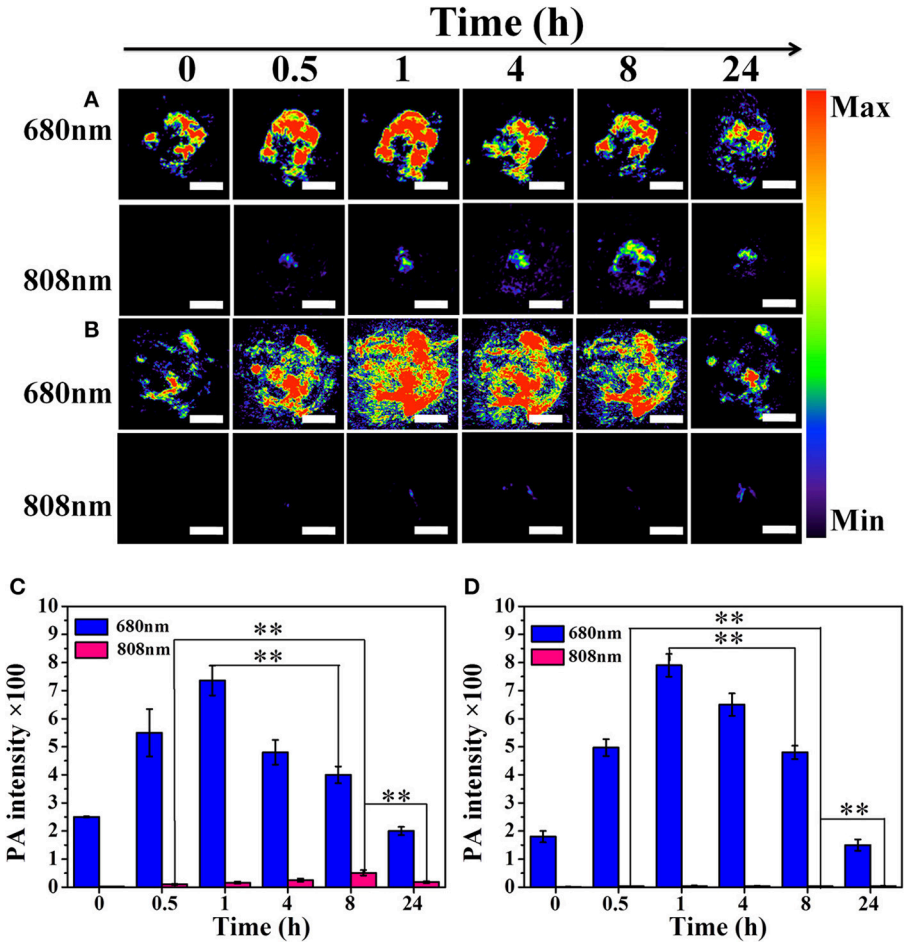

FIGURE 8 | *In vivo* the photoacoustic imaging (PA) of tumor-bearing mice at 0/0.5/1/4/8/24 h after intravenous injection. **(A)** Cy-SS-MTX excited by 680 nm and 808 nm respectively. **(B)** Cy-CC-MTX excited by 680 nm and 808 nm respectively. **(C)** Semiquantitative average PA signals in the tumor site of **(A)**. **(D)** Semiquantitative average PA signals in the tumor site of **(B)**. Red PA signals excited by 745 nm represent the drug release. (100 μl, 80 μg/ml for each mice, Scale bar of **A,B**: 5 mm). (*denotes $P < 0.05$, **denotes $P < 0.01$ significant difference).

average FL signals of Cy-SS-MTX and Cy-CC-MTX also directly showed the above trends (**Figures 8C,D**). The data indicated that Cy-SS-MTX could rapidly target tumor. Besides, the signals of PA imaging excited by 808 nm of Cy-SS-MTX had an increasing trend within 8 h and then gradual decreasing, but the signals of Cy-CC-MTX had no almost changing signal. The changing signals of PA imaging further certificated that the activation of prodrug Cy-SS-MTX could also be checked with PA imaging. The aforementioned results confirmed that the activation of prodrug *in vivo* could be monitored by 640/745 nm excitation for FL imaging, and 680/808 nm excitation for PA imaging.

CONCLUSION

We have developed a novel SCTPs Cy-SS-MTX based on heptamethine cyanine dye as reporter group. The presence of GSH in tumor could activate prodrug and change the optical properties of Cy group in prodrug. Under different excitation wavelengths, we could real-timely track the activation of prodrug by FL/PA dual-modal imaging. Moreover, the prodrug apparently improved anti-tumor efficiency of MTX to cancer cells and significantly reduced its toxicity to normal cells. This strategy may offer an approach for the development of SCTPs to improve therapeutic effect and reduce toxicity of traditional anti-cancer drugs.

AUTHOR CONTRIBUTIONS

SL and ZS made common efforts in finishing the experiment. XM and GD provided some guidance in technology. JZ and KZ checked our paper in writing. WL and LZ provided some helps in cell experiments. PG and LC supervised the work.

ACKNOWLEDGMENTS

This work was financially supported by Key International S&T Cooperation Project (2015DFH50230), the NSF of

China (No. 21375141, 81671758, and 31571013), Guangdong NSF of Research Team (2016A030312006) and Shenzhen Science and Technology Program (JSGG201603311854 22390, JCYJ20160429191503002, JCYJ20170818162522 440).

SUPPLEMENTARY MATERIAL

The Supplementary Material for this article can be found online at: https://www.frontiersin.org/articles/10.3389/fmats.2018.00035/full#supplementary-material

REFERENCES

Abet, V., Filace, F., Recio, J., Alvarez-Builla, J., and Burgos, C. (2017). Prodrug approach: an overview of recent cases. *Eur. J. Med. Chem.* 127, 810–827. doi: 10.1016/j.ejmech.2016.10.061

Atchison, J., Kamila, S., Nesbitt, H., Logan, K. A., Nicholas, D. M., Fowley, C., et al. (2017). Iodinated cyanine dyes: a new class of sensitisers for use in NIR activated photodynamic therapy (PDT). *Chem. Commun. (Camb).* 53, 2009–2012. doi: 10.1039/C6CC09624G

Beard, P. (2011). Biomedical photoacoustic imaging. *Interface Focus* 1, 602–631. doi: 10.1098/rsfs.2011.0028

Bi, Y., Liu, L., Lu, Y., Sun, T., Shen, C., Chen, X., et al. (2016). T7 peptide-functionalized PEG-PLGA micelles loaded with carmustine for targeting therapy of glioma. *ACS Appl. Mater. Interfaces* 8, 27465–27473. doi: 10.1021/acsami.6b05572

Chao, S., Krejci, E., Bernard, V., Leroy, J., Jean, L., and Renard, P. Y. (2016). A selective and sensitive near-infrared fluorescent probe for acetylcholinesterase imaging. *Chem. Commun. (Camb).* 52, 11599–11602. doi: 10.1039/C6CC05936H

Don, T. M., Lu, K. Y., Lin, L. J., Hsu, C. H., Wu, J. Y., and Mi, F. L. (2017). Temperature/pH/enzyme triple-responsive cationic protein/PAA-b-PNIPAAm nanogels for controlled anticancer drug and photosensitizer delivery against multidrug resistant breast cancer cells. *Mol. Pharm.* 14, 4648–4660. doi: 10.1021/acs.molpharmaceut.7b00737

Gangopadhyay, M., Mengji, R., Paul, A., Venkatesh, Y., Vangala, V., Jana, A., et al. (2017). Redox-responsive xanthene–coumarin–chlorambucil-based FRET-guided theranostics for "activatable" combination therapy with real-time monitoring. *Chem. Commun.* 53, 9109–9112. doi: 10.1039/c7cc03241b

Gao, M., Yu, F., Lv, C., Choo, J., and Chen, L. (2017). Fluorescent chemical probes for accurate tumor diagnosis and targeting therapy. *Chem. Soc. Rev.* 46, 2237–2271. doi: 10.1039/C6CS00908E

Guan, Y., Zhang, Y., Xiao, L., Li, J., Wang, J. P., Chordia, M. D., et al. (2017). Improving therapeutic potential of farnesylthiosalicylic acid: tumor specific delivery via conjugation with heptamethine cyanine dye. *Mol. Pharm.* 14, 1–13. doi: 10.1021/acs.molpharmaceut.5b00906

Han, H., Valdepérez, D., Jin, Q., Yang, B., Li, Z., Wu, Y., et al. (2017). Dual enzymatic reaction-assisted gemcitabine delivery systems for programmed pancreatic cancer therapy. *ACS Nano* 11, 1281–1291. doi: 10.1021/acsnano.6b05541

He, L., Yang, X., Xu, K., Kong, X., and Lin, W. (2017). A multi-signal fluorescent probe for simultaneously distinguishing and sequentially sensing cysteine/homocysteine, glutathione, and hydrogen sulfide in living cells. *Chem. Sci.* 8, 6257–6265. doi: 10.1039/C7SC00423K

Hu, X., Hu, J., Tian, J., Ge, Z., Zhang, G., Luo, K., et al. (2013). Polyprodrug amphiphiles: hierarchical assemblies for shape-regulated cellular internalization, trafficking, and drug delivery. *J. Am. Chem. Soc.* 135, 17617–17629. doi: 10.1021/ja409686x

Hu, Y. Q., Xu, Z., Zhang, S., Wu, X., Ding, J. W., Lv, Z. S., et al. (2017). Recent developments of coumarin-containing derivatives and their anti-tubercular activity. *Eur. J. Med. Chem.* 136, 122–130. doi: 10.1016/j.ejmech.2017.05.004

Huttunen, K. M., Raunio, H., and Rautio, J. (2011). Prodrugs–from serendipity to rational design. *Pharmacol. Rev.* 63, 750–771. doi: 10.1124/pr.110.003459

Jeon, M., Kim, J., and Kim, C. (2014). Multiplane spectroscopic whole-body photoacoustic imaging of small animals *in vivo*. *Med. Biol. Eng. Comput.* 54, 283–294. doi: 10.1007/s11517-014-1182-6

Kang, M. S., Singh, R. K., Kim, T. H., Kim, J. H., Patel, K. D., and Kim, H.-W. (2017). Optical imaging and anticancer chemotherapy through carbon dot created hollow mesoporous silica nanoparticles. *Acta Biomater.* 55, 466–480 doi: 10.1016/j.actbio.2017.03.054

Kumar, R., Shin, W. S., Sunwoo, K., Kim, W. Y., Koo, S., Bhuniya, S., et al. (2015). Small conjugate-based theranostic agents: an encouraging approach for cancer therapy. *Chem. Soc. Rev.* 44, 6670–6683. doi: 10.1039/C5CS00224A

Lee, M. H., Sharma, A., Chang, M. J., Lee, J., Son, S., Sessler, J. L., et al. (2017). Fluorogenic reaction-based prodrug conjugates as targeted cancer theranostics. *Chem. Soc. Rev.* **47**, 28–52. doi: 10.1039/c7cs00557a

Li, B., Liu, P., Yan, D., Zeng, F., and Wu, S. (2017). A self-immolative and DT-diaphorase-activatable prodrug for drug-release tracking and therapy. *J. Mater. Chem. B* 5, 2635–2643. doi: 10.1039/C7TB00266A

Li, S. Y., Liu, L. H., Jia, H. Z., Qiu, W. X., Rong, L., Cheng, H., et al. (2014). A pH-responsive prodrug for real-time drug release monitoring and targeted cancer therapy. *Chem. Commun. (Camb).* 50, 11852–11855. doi: 10.1039/C4CC05008H

Li, Y., Lin, J., Wu, H., Chang, Y., Yuan, C., Liu, C., et al. (2015). Orthogonally Functionalized nanoscale micelles for active targeted codelivery of methotrexate and mitomycin C with synergistic anticancer effect. *Mol. Pharm.* 12, 769–782. doi: 10.1021/mp5006068

Li, Y., Liu, W., Zhang, P., Zhang, H., Wu, J., Ge, J., et al. (2017). A fluorescent probe for the efficient discrimination of Cys, Hcy and GSH based on different cascade reactions. *Biosens. Bioelectron.* 90, 117–124. doi: 10.1016/j.bios.2016.11.021

Lim, E. K., Kim, T., Paik, S., Haam, S., Huh, Y. M., and Lee, K. (2014). Nanomaterials for theranostics: recent advances and future challenges. *Chem. Rev.* 115, 327–394. doi: 10.1021/cr300213b

Lin, J., Li, Y., Li, Y., Cui, F., Yu, F., Wu, H., et al. (2015). Self-targeted, bacillus-shaped, and controlled-release methotrexate prodrug polymeric nanoparticles for intratumoral administration with improved therapeutic efficacy in tumor-bearing mice. *J. Mater. Chem. B* 3, 7707–7717. doi: 10.1039/C5TB00724K

Liu, P., Li, B., Zhan, C., Zeng, F., and Wu, S. (2017). A two-photon-activated prodrug for therapy and drug release monitoring. *J. Mater. Chem. B* 5, 7538–7546. doi: 10.1039/C7TB01408B

Liu, P., Xu, J., Yan, D., Zhang, P., Zeng, F., Li, B., et al. (2015). A DT-diaphorase responsive theranostic prodrug for diagnosis, drug release monitoring and therapy. *Chem. Commun.* 51, 9567–9570. doi: 10.1039/C5CC02149A

Liu, P., Yue, C., Shi, B., Gao, G., Li, M., Wang, B., et al. (2013). Dextran based sensitive theranostic nanoparticles for near-infrared imaging and photothermal therapy *in vitro*. *Chem. Commun. (Camb).* 49, 6143–6145. doi: 10.1039/c3cc43633k

Meng, X., Yang, Y., Zhou, L., Zhang, L., Lv, Y., Li, S., et al. (2017). Dual-responsive molecular probe for tumor targeted imaging and photodynamic therapy. *Theranostics* 7, 1781–1794. doi: 10.7150/thno.18437

Mitcham, T., Dextraze, K., Taghavi, H., Melancon, M., and Bouchard, R. (2015). Photoacoustic imaging driven by an interstitial irradiation source. *Photoacoustics* 3, 45–54. doi: 10.1016/j.pacs.2015.02.002

Morsy, S. A., Farahat, A. A., Nasr, M. N. A., and Tantawy, A. S. (2017). Synthesis, molecular modeling and anticancer activity of new coumarin containing compounds. *Saudi Pharm. J.* 25, 873–883. doi: 10.1016/j.jsps.2017.02.003

Penet, M. F., Chen, Z., Li, C., Winnard, P. T., and Bhujwalla, Z. M. (2012). Prodrug enzymes and their applications in image-guided therapy of cancer: tracking prodrug enzymes to minimize collateral damage. *Drug Deliv. Transl. Res.* 2, 22–30. doi: 10.1007/s13346-011-0052-0

Rautio, J., Kumpulainen, H., Heimbach, T., Oliyai, R., Oh, D., Järvinen, T., et al. (2008). Prodrugs: design and clinical applications. *Nat. Rev. Drug Discov.* 7, 255–270. doi: 10.1038/nrd2468

Shi, C., Wu, J. B., and Pan, D. (2016). Review on near-infrared heptamethine cyanine dyes as theranostic agents for tumor imaging, targeting, and photodynamic therapy. *J. Biomed. Opt.* 21:50901. doi: 10.1117/1.JBO.21.5.050901

Sun, W., Guo, S., Hu, C., Fan, J., and Peng, X. (2016). Recent development of chemosensors based on cyanine platforms. *Chem. Rev.* 116, 7768–7817. doi: 10.1021/acs.chemrev.6b00001

Tam, Y. T., Gao, J., and Kwon, G. S. (2016). Oligo(lactic acid)n-paclitaxel prodrugs for poly(ethylene glycol)-block-poly(lactic acid) micelles: loading, release, and backbiting conversion for anticancer activity. *J. Am. Chem. Soc.* 138, 8674–8677. doi: 10.1021/jacs.6b03995

Tibbitt, M. W., Dahlman, J. E., and Langer, R. (2016). Emerging frontiers in drug delivery. *J. Am. Chem. Soc.* 138, 704–717. doi: 10.1021/jacs.5b09974

Warnecke, A., Fichtner, I., Sass, G., and Kratz, F. (2007). Synthesis, cleavage profile, and antitumor efficacy of an albumin-binding prodrug of methotrexate that is cleaved by plasmin and cathepsin B. *Arch. Pharm. (Weinheim).* 340, 389–395. doi: 10.1002/ardp.200700025

Wu, J. B., Lin, T. P., Gallagher, J. D., Kushal, S., Chung, L. W., Zhau, H. E., et al. (2015a). Monoamine oxidase A inhibitor-near-infrared dye conjugate reduces prostate tumor growth. *J. Am. Chem. Soc.* 137, 2366–2374. doi: 10.1021/ja512613j

Wu, J. B., Shi, C., Chu, G. C., Xu, Q., Zhang, Y., Li, Q., et al. (2015b). Near-infrared fluorescence heptamethine carbocyanine dyes mediate imaging and targeted drug delivery for human brain tumor. *Biomaterials* 67, 1–10. doi: 10.1016/j.biomaterials.2015.07.028

Wu, X., Sun, X., Guo, Z., Tang, J., Shen, Y., James, T. D., et al. (2014). *In vivo* and *in situ* tracking cancer chemotherapy by highly photostable NIR fluorescent theranostic prodrug. *J. Am. Chem. Soc.* 136, 3579–3588. doi: 10.1021/ja412380j

Ye, M., Wang, X., Tang, J., Guo, Z., Shen, Y., Tian, H., et al. (2016). Dual-channel NIR activatable theranostic prodrug for *in vivo* spatiotemporal tracking thiol-triggered chemotherapy. *Chem. Sci.*. 7, 4958–4965. doi: 10.1039/C6SC00970K

Zhang, Y., Hong, H., and Cai, W. (2011). Photoacoustic Imaging. *Cold Spring Harb. Protoc.* 2011:pdb.top065508. doi: 10.1101/pdb.top065508

Zhao, X., Li, Y., Jin, D., Xing, Y., Yan, X., and Chen, L. (2015). A near-infrared multifunctional fluorescent probe with an inherent tumor-targeting property for bioimaging. *Chem. Commun. (Camb).* 51, 11721–11724. doi: 10.1039/C5CC03878B

Zheng, M., Wang, Y., Shi, H., Hu, Y., Feng, L., Luo, Z., et al. (2016). Redox-mediated disassembly to build activatable trimodal probe for molecular imaging of biothiols. *ACS Nano* 10, 10075–10085. doi: 10.1021/acsnano.6b05030

Zhou, Z., Jafari, M., Sriram, V., Kim, J., Lee, J. Y., Ruiz-Torres, S. J., et al. (2017). Delayed sequential co-delivery of gefitinib and doxorubicin for targeted combination chemotherapy. *Mol. Pharm.* 14, 4551–4559. doi: 10.1021/acs.molpharmaceut.7b00669

Conflict of Interest Statement: The authors declare that the research was conducted in the absence of any commercial or financial relationships that could be construed as a potential conflict of interest.